JOURNAL OF VIROLOGY, Oct. 2009, p. 10504–10514 Vol. 83, No. 20
0022-538X/09/$08.00+0 doi:10.1128/JVI.00295-09

Early Steps in Cell Infection by Parvoviruses: Host-Specific Differences in Cell Receptor Binding but Similar Endosomal Trafficking▽†

Carole E. Harbison, Sangbom Michael Lyi, Wendy S. Weichert, and Colin R. Parrish*

Baker Institute for Animal Health, Department of Microbiology and Immunology, College of Veterinary Medicine, Cornell University, Ithaca, New York 14853

Received 11 February 2009/Accepted 26 July 2009

Canine parvovirus (CPV) and feline panleukopenia virus (FPV) are closely related parvoviruses that differ in their host ranges for cats and dogs. Both viruses bind their host transferrin receptor (TfR), enter cells by clathrin-mediated endocytosis, and traffic with that receptor through endosomal pathways. Infection by these viruses appears to be inefficient and slow, with low numbers of virions infecting the cell after a number of hours. Species-specific binding to TfR controls viral host range, and in this study FPV and strains of CPV differed in the levels of cell attachment, uptake, and infection in canine and feline cells. During infection, CPV particles initially bound and trafficked passively on the filopodia of canine cells while they bound to the cell body of feline cells. That binding was associated with the TfR as it was disrupted by anti-TfR antibodies. Capsids were taken up from the cell surface with different kinetics in canine and feline cells but, unlike transferrin, most did not recycle. Capsids labeled with fluorescent markers were seen in Rab5-, Rab7-, or Rab11-positive endosomal compartments within minutes of uptake, but reached the nucleus. Constitutively active or dominant negative Rab mutants changed the intracellular distribution of capsids and affected the infectivity of virus in cells.

Cell infection by animal viruses involves a specific sequence of steps that deliver the virus and its genome from the cell surface to the compartment where replication can occur. For nonenveloped viruses, infection initiates with binding to a specific cell receptor and uptake into the cell by receptor-mediated endocytosis. Various factors can control the process of viral uptake, including the characteristics of the receptor(s) bound by the virus and its signaling and endocytic properties, the affinity of the virus for the receptor, and the structural features of the interaction in different environments (36, 61). Receptors may be located on the cell body or may also be displayed on the extended lamellipodia or filopodia with greater surface areas. Viruses binding to filopodia can be either passively delivered to the cell body for endocytosis by dynamic movement of the entire structure or actively trafficked by retrograde actin transport as well as the action of myosin-2 motors on the actin (32, 57). Cross-linking and clustering of receptors by viral particles can influence the rate and pathways of uptake from the cell surface (23), and many viral receptors activate signaling pathways that alter the structure of the underlying cytoskeleton to enhance uptake (see, e.g., references 12, 30, and 51). Receptor-bound viruses then enter one or more endosomal pathways that results in the capsid being enclosed in vesicles and trafficked within the endosomal pathways of the cell, where clustered virus and receptors (23) may undergo structural alterations upon exposure to conditions such as low pH or proteases (36, 61). The specific receptor-mediated binding and entry pathways often provide signals for viruses that allow endosomal escape and establish infection. A variety of markers of the endosomal compartments have been used in studies of viral entry. Rab proteins are monomeric small GTPases which regulate endosomal membrane trafficking, and specific Rab proteins are associated with different endosomal compartments. Among the many Rab proteins in the cells, Rab5 is primarily associated with the early endosome and regulates trafficking through that compartment, Rab7 is associated with the late endosome, and Rab11 is associated with the recycling endosome (14, 58). Tracking viral particles within the endosomal pathways during cell entry has been used to define the steps in the entry and infection processes of a variety of different viruses and has revealed many of the common features and variant processes that are used (7–9, 33, 71).

Here, we examine the uptake and infection of cells by parvovirus capsids and compare some of the steps followed by capsids that differ in their receptor binding properties and host ranges. Feline panleukopenia virus (FPV) infects cats (50, 66), binds the transferrin receptor-1 (TfR) on feline cells, and uses that receptor for uptake and infection (27, 44). FPV does not bind the canine TfR or infect dogs or cultured canine cells. Canine parvovirus (CPV) is a natural variant of FPV which emerged in 1978 after acquiring a small number of mutations that allow its capsid to bind the canine TfR (27). The original strain of CPV (designated CPV type 2 [CPV-2]) spread worldwide in dogs during 1978, but some of the same mutations that gave it the canine host range rendered it unable to infect cats (66, 67). CPV-2 was replaced worldwide during 1979 and 1980 by a natural variant, CPV type 2a (CPV-2a), which contained an additional four to five changes in its coat protein gene (48, 49). Subsequently, the canine viruses have continued to evolve, and additional single mutations have been selected that alter antigenic epitopes. Strains altered at VP2 residue 426 are des-

* Corresponding author. Mailing address: Baker Institute for Animal Health, Department of Microbiology and Immunology, College of Veterinary Medicine, Cornell University, Ithaca, NY 14853. Phone: (607) 256-5649. Fax: (607) 256-5608. E-mail: crp3@cornell.edu.

† Supplemental material for this article may be found at http://jvi.asm.org/.

▽ Published ahead of print on 5 August 2009.

ignated CPV-2b (Asn426Asp) and CPV-2c (Asp426Glu) (13, 48). CPV-2a and its variants are able to infect both dogs and cats but show reduced binding to the feline TfR on cells and in vitro (27, 42). In addition, the affinity of binding to the canine TfR is much lower than that seen for the feline TfR (42).

The TfR is a type II membrane protein expressed in nonlipid raft regions of the plasma membrane, and it binds iron-loaded (holo) transferrin (Tf) at neutral pH (2). TfR expression is tightly regulated, and it is more highly expressed on dividing cells with high iron needs, which would favor binding of these viruses. The TfRs of mice and humans are used as receptors for cell infection by the mouse mammary tumor virus and the New World hemorrhagic fever arenaviruses (52, 56).

The TfR is assembled as a homodimer, and each monomer of the ectodomain is composed of protease-like, apical and helical domains, as well as a 30-Å membrane-proximal stalk (5, 20, 31). The transmembrane domain mediates membrane insertion and influences some aspects of trafficking within the cell, while the cytoplasmic domain contains a tyrosine-threonine-arginine-phenylalanine (YTRF) sequence that engages the clathrin-mediated endocytic machinery through AP-2 (adaptor protein-2) (53, 55). The TfR sequence also includes one or two cysteines adjacent to the inner leaflet of the membrane that may be palmitoylated to influence the rate of receptor recycling, and it also contains sequences that control basolateral localization in polarized cells (41). In the normal pathway of TfR-mediated entry, the TfR-holo-Tf complex is transported into the endosomal system, where low pH results in conformational changes and iron release. The TfR-Tf complex enters the early endosome, from which some of the complex is rapidly recycled to the cell surface while most passes to the perinuclear recycling endosome. From there it recycles to the cell surface where the iron-free apo-Tf is released at neutral pH (21, 22, 24, 37, 38, 69, 70). The rate of uptake and the efficiency of TfR recycling depend on the form of the ligand, and more than 97% of monomeric Tf recycles to the cell surface within 10 to 30 min. However, cross-linking TfRs with oligomeric Tf or antibodies causes the complexes to be retained within endosomes for longer times, and a higher proportion is trafficked to late endosomes and lysosomes for degradation (35).

Holo-Tf binds the membrane-proximal side of the feline and canine TfR ectodomain (11), while virus binding involves the apical domain of the receptor as mutations in that structure affect the ability to bind FPV and CPV capsids (43) The feline and canine TfRs differ in ~10% of their sequences, but a major difference controlling the CPV-specific binding is a unique glycosylation site in the apical domain of the canine TfR (43). Alteration of the glycosylated Asn to Lys (the feline TfR residue) allowed the canine TfR to bind FPV and also greatly increased the affinity of binding to CPV-2 and CPV-2a-related capsids (42).

CPV and FPV have small (25 nm) nonenveloped capsids that package a single-stranded DNA genome of ~5,120 bases (68). The particles are made up of two overlapping proteins, VP1 and VP2, with 90% of the capsid protein being VP2. VP1 contains a 143-residue amino (N)-terminal sequence that encodes a phospholipase A_2 enzymatic activity, as well as basic amino acid motifs that play a role in nuclear localization (72). The VP1 unique region becomes exposed during cell entry without capsid disintegration, and the phospholipase A_2 modifies the endosomal membrane to enhance endosomal escape (19, 75).

Previous studies of cell entry by CPV, minute virus of mice, and various adeno-associated viruses (AAVs) show that viral uptake primarily occurs through clathrin-mediated endocytosis. However, when the AP-2-interacting sequences in the cytoplasmic tail of the feline TfR were mutated or deleted, the altered receptor still allowed CPV infection at a similar efficiency to that of wild-type TfR (26). The intracellular pathways of viral entry and trafficking have been examined by using cells fixed at various times after uptake and then antibody stained for virus and cellular markers or by expressing green fluorescent protein (GFP)-labeled markers. Time courses examined were between 1 and 6 h, and sequential steps of trafficking were suggested, with the virus passed from the early endosomes to the recycling endosome, followed by localization in late endosomes and lysosomes after uptake (65). By fluorescent antibody staining, VP1 release occurred only hours after uptake, possibly in a low-pH degradative compartment (64, 72). In addition, CPV capsids appear to remain associated with the receptor for 1 to 2 h after virus uptake as antibodies against the TfR cytoplasmic tail microinjected into feline CRFK cells block infection in this time period (44). Infection is also blocked by neutralizing the low pH of the endosomal system with ammonium chloride or bafilomycin A1, although it is not clear whether this is due to direct effects on the capsid or to indirect alterations in endosomal trafficking. When the X-ray crystal structures of capsids of CPV and FPV were determined at low pH or in the presence of EDTA or when capsids were examined for changes in protease susceptibility, only small changes in surface loops of the viral structure were present (40, 60).

Here, we used microscopy to examine dynamic steps in the binding, uptake, and early trafficking of parvovirus capsids in live canine and feline cells. Labeled capsids were seen to undergo rapid movement into multiple endosomal compartments shortly after entry. Initial binding of CPV to canine cells involved filopodia while in feline cells the virus bound primarily to receptors on the cell body. In cells expressing GFP-conjugated Rab proteins, particles rapidly localized to multiple endosomal compartments in the cytoplasm after uptake, which gradually accumulated near the microtubule-organizing center. The distribution of intracellular viruses and the viral infectivity in feline cells were altered by expression of either constitutively active (CA) or dominant negative (DN) mutants of the Rab proteins.

MATERIALS AND METHODS

Cells and viruses. Feline CRFK and NLFK cells and canine A72 and Cf2Th cells were grown in a 1:1 mixture of McCoy's 5A and Liebovitz L15 media with 5% fetal bovine serum. Chinese hamster ovary-derived cells lacking the hamster TfR (TRVb cells) (39) were grown in Ham's F12 medium containing 5% fetal bovine serum.

Viruses were derived from infectious plasmid clones of FPV (FPV-b), CPV-2 (CPV-d), and CPV-2b (CPV-39) strains (27, 47). Plasmids were transfected into NLFK cells, and the viruses recovered were titrated using 50% tissue culture infective dose ($TCID_{50}$) assays (46). Virus capsids were concentrated by polyethylene glycol precipitation, followed by sucrose gradient centrifugation, and

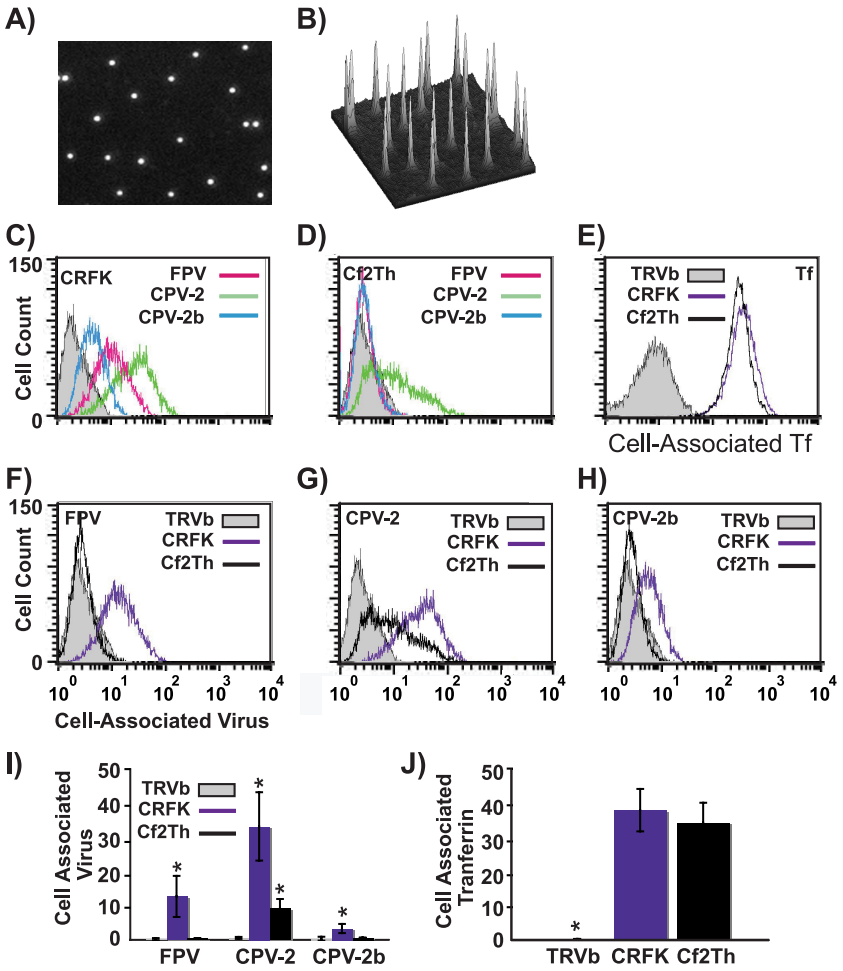

FIG. 1. (A and B) Analysis of Alexa Fluor 594-labeled CPV-2 full capsids by fluorescence microscopy. Diluted virus was sandwiched between two coverslips and imaged with a 100× oil lens (A). Panel B shows the intensity of the fluorescence associated with the particles shown in panel A. (C to E) Labeled capsids associated with canine or feline cells, determined by flow cytometry. The amount of FPV, CPV-2, or CPV-2b that bound and was taken up into feline CRFK cells (C) or canine Cf2Th cells (D) after 1 h at 37°C is shown. Panel E shows canine Tf incubated with canine and feline cells under the same conditions. TRVb cells expressing no TfR were used as a negative control for all assays. (F to H) The same data are represented to allow comparison between binding and uptake of FPV, CPV-2, and CPV-2b capsids in feline or canine cells. (I and J) The mean and standard deviation (from three independent experiments) of the background-subtracted mean fluorescence intensities, showing binding and uptake of the three viruses or canine Tf. (*, $P < 0.05$).

then dialyzed against either phosphate-buffered saline (PBS) or 20 mM Tris-HCl (pH 7.5) and stored at 4°C (1, 40).

Fluorescent markers and ligands, fluorescence microscopy, and intracellular localization. Rab5, Rab11, and Rab7 genes with GFP fused to the N termini were obtained from Craig Roy, Yale University, or in some cases prepared by site-directed mutagenesis. CA mutants included Rab5-Q79L, Rab7-Q67L, and Rab11-Q70V, and DN mutants were Rab5-S34N, Rab7-T22N, and Rab11-S25N. Cells were transfected with plasmid DNA using Lipofectamine (Invitrogen, San Diego, CA) and 2 days later were seeded in culture dishes with coverslip inserts for imaging (MatTek, Ashland, MA).

Canine Tf (Sigma) was iron loaded as previously described (4). Purified CPV capsids, FPV capsids, or canine Tf were labeled with Alexa Fluor 488, Alexa Fluor 594, or Alexa Fluor 647 dyes (Invitrogen) at 20% of the recommended concentrations for 30 min at 21°C (27). The labeled capsids or Tf were dialyzed extensively against 0.2 M PBS at pH 8.2, passed through a P10 gel filtration column (Millipore, Billerica, MA), and stored at 4°C. Capsids were examined by fluorescence microscopy, and images collected were analyzed with ImageJ software (U.S. National Institutes of Health, Bethesda, MD).

Cells were incubated at 37°C for 5 min with either labeled capsids or labeled Tf, the medium was replaced with phenol red-free Dulbecco's modified Eagle medium, and the cells were observed using a 100× oil lens at 37°C and time-lapse imaging. Images were collected with a Hamamatsu OrcaER charge-coupled-device camera, with different labels collected sequentially as separate channels. Images were analyzed using SimplePCI (Hamamatsu, Sewickley, PA). Colocalization of the virions and endosomal markers was determined with ImageJ software, and particle tracking was performed using the ImageJ manual tracker plug-in (Institut Curie, Orsay, France). Confocal images were obtained from live cells using a Zeiss LSM510 confocal microscope, and images were prepared and analyzed using Zeiss ZEN 2008 software.

For intracellular actin Alexa Fluor 488-labeled actin from rabbit muscle (Molecular Probes, Eugene, OR) was injected into cells at a concentration of 1 mg/ml using an Eppendorf injector and micromanipulator. Cells were incubated at 37°C for 60 min to allow actin diffusion and incorporation into cellular structures, and then Alexa Fluor 594-labeled CPV-2 capsids were added and visualized as described above. In other cases cells were transfected with plasmids expressing actin-GFP or lamin-A/C-GFP.

To determine the specific role of the TfR in virus or Tf binding to the cells, antibodies against the cytoplasmic tail or the ectodomain of the receptor were used. Antibody H68.4 (Zymed, South San Francisco, CA) recognizes the cytoplasmic tail of the TfR, and that was injected into cells using an Eppendorf microinjector and micromanipulator 30 min prior to incubating the cells with virus or Tf. Rabbit antibodies against the extracellular domain of the receptor were prepared from the peptide at residues 559 to 571 of the human TfR after being conjugated to keyhole limpet hemocyanin (42).

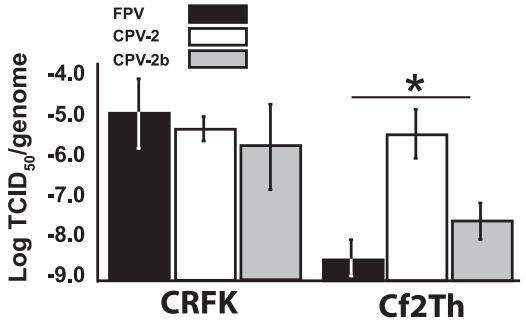

FIG. 2. Relative infectivities of FPV, CPV-2, or CPV-2b samples when inoculated into canine and feline cells, showing the mean log $TCID_{50}$/genome. The mean ± 1 standard deviation from three independent experiments is shown (*, $P < 0.05$).

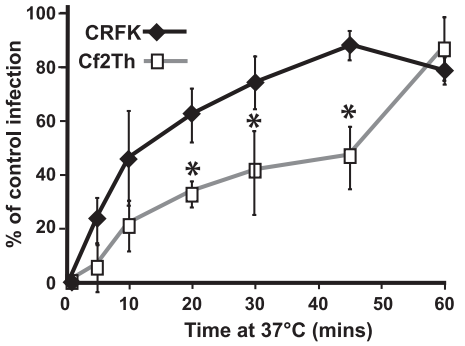

FIG. 3. Kinetics of uptake and infection of CPV-2 in feline and canine cells. The percentage of infecting virus that resisted antibody neutralization at various times after virus binding to feline CRFK or canine Cf2th cells was compared to control infections where no antibody was added (*, $P < 0.05$ for differences between feline and canine cells).

Virus or Tf cell binding, uptake, and recycling. Cell-associated Alexa Fluor 488-labeled virus or Alexa Fluor 647-labeled Tf was analyzed with a FACSCalibur flow cytometer and Cell Quest software (Becton-Dickinson, San Jose, CA). Cells cultured in 10-cm^2 dishes overnight were incubated with 10 μg/ml labeled ligand for 1 h at 37°C. After two washes in Hank's buffered saline solution without Mg^{2+} or Ca^{2+}, cells were detached using 1 mM EDTA in Hank's buffered saline solution on ice and then fixed with 4% paraformaldehyde in PBS prior to analysis. One- and two-tailed Student's *t* tests were performed to assess the differences between the geometric mean fluorescence intensity levels after background subtraction.

To examine the recycling of capsids or Tf, Alexa Fluor 488-labeled virus or Alexa Fluor 647-Tf was bound to CRFK or Cf2Th cells on ice for 30 min. The cells were warmed to 37°C, and the relative amounts of cell-associated capsids or Tf were determined at various times of incubation as above.

Cell infection assays and relative infectivity. $TCID_{50}$ titers were determined for freshly prepared stocks of the FPV, CPV-2, and CPV-2b strains of virus in CRFK and Cf2Th cells as previously described (46). The amount of viral single-stranded DNA in each inoculum was determined by quantitative PCR using a SYBR Green 1-labeled probe (Applied Biosystems, Foster City, CA) and was standardized using known samples of the cloned CPV-2 genome. Student's *t* tests and paired *t* tests were used where indicated to examine the differences between the log $TCID_{50}$/genome results.

Time course of infection. The rate of virus uptake was determined by measuring the infectivity in cells treated with neutralizing rabbit anti-CPV antiserum added at various times after inoculation (45). Cells seeded at 2×10^4 cells/cm^2 were cultured overnight. The viruses were diluted in Dulbecco's modified Eagle medium with 0.1% bovine serum albumin and incubated with the cells for 30 min on ice. The cells were cultured at 37°C in growth medium, and at various times medium containing a 1:1,000 dilution of a rabbit anti-CPV serum was added. After 24 h, cells were fixed with 4% paraformaldehyde and stained with an anti-NS1 antibody (CE 10) (74) and an Alexa Fluor 488-labeled goat anti-mouse immunoglobulin G secondary antibody.

RESULTS

Cell binding levels. Labeled virus particles showed an even distribution of apparent single particles, with similar levels of labeling (Fig. 1A and B), and they banded on sucrose gradients at positions expected for full particles (results not shown). The amounts of labeled viruses binding to the canine or feline cells tested depended on the specific combination of virus strain and host cell (Fig. 1). All viruses bound and entered feline cells (Fig. 1C), though to different levels. Levels of binding and uptake seen were similar to those seen for unlabeled viruses that were subsequently detected with antibodies (27). Although CPV-2 and CPV-2b both infected canine cells, the level of CPV-2b binding was close to background levels, likely due to the low affinity of this interaction (Fig. 1D and H) (42). Feline cells bound and endocytosed CPV-2 and CPV-2b capsids to 3.5- and 5-fold higher levels, respectively, than canine cells (Fig. 1G and H). Comparing different viral strains showed that CPV-2 capsids bound to ~10-fold higher levels than CPV-2b capsids in all cell lines tested (Fig. 1C, D, and I). In feline cells, FPV had an intermediate level of binding and uptake compared to the two CPV strains. These differences were not related to the levels of TfR expression as both the CRFK and Cf2Th cells bound equivalent amounts of canine Tf while the TfR-negative TRVb cells bound neither virus nor Tf (Fig. 1E and 1J).

Infectivity of viruses in canine and feline cells. The relative infectivity of FPV, CPV-2, and CPV-2b, determined as log $TCID_{50}$/genome, varied between cell lines (Fig. 2). Two canine and two feline cell lines were tested with two separately prepared inocula of each virus, and similar patterns were seen for each host type. Data from one inoculum in one cell line per species is shown in Fig. 2. CPV-2 had equal infectivity in canine and feline cells while FPV and CPV-2b were significantly more infectious in feline than in canine cells. About 1×10^5 virions were needed to infect CRFK cells, with no significant differences in infectivity between the three virus strains. CPV-2 was up to 100-fold more infectious than CPV-2b on a per-genome basis in Cf2th canine cells while FPV showed only background levels of infection in those cells.

Uptake from the cell surface. Antibody neutralization of extracellular virus was used to determine the rate of uptake from the surface of feline and canine cells. The infecting viruses rapidly acquired resistance to neutralization in feline cells, with CPV-2 infection levels reaching 50% of control levels within 10 min of warming to 37°C. The uptake into canine cells was slower, taking 45 min to reach 50% protection of the virus (Fig. 3).

Fluorescence microscopy was used to follow the capsids into cells. Purified full capsids were labeled with Alexa Fluor dyes to a ratio of 5 to 12 mol of dye molecules per capsid (Fig. 1A and B). In general the labeled capsids showed similar overall uptake patterns of cell binding and entry to those reported for unlabeled capsids examined after fixing and antibody staining, but there was more resolution in terms of special distribution over time (65). The labeled capsids had similar levels of infectivity (data not shown;).

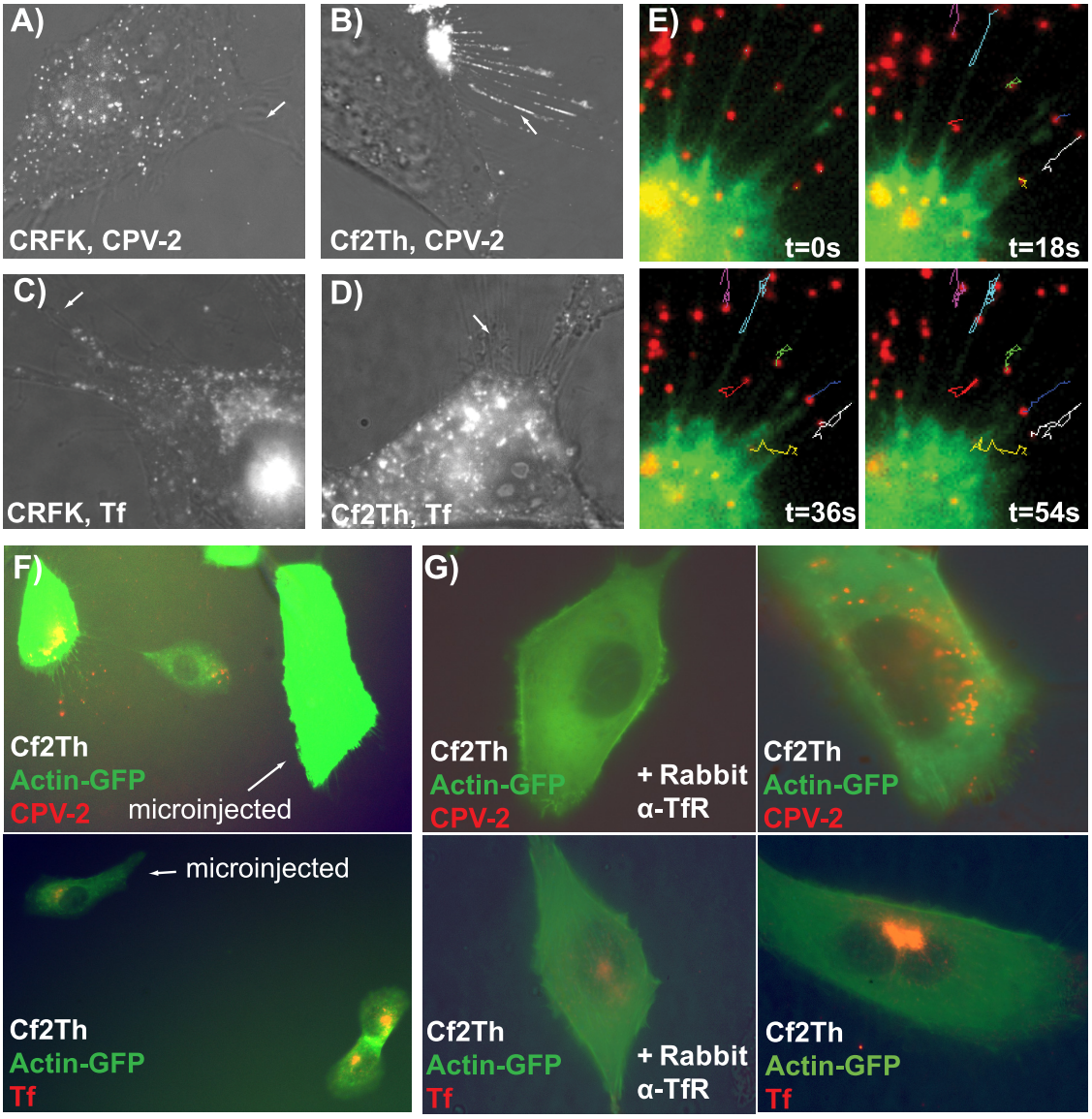

FIG. 4. Association of CPV-2 with filopodia on canine or feline cells. Alexa Fluor 594-labeled capsids were incubated with feline (A) or canine (B) cells for 5 min at 37°C and then observed immediately. Alexa Fluor 594-Tf was also incubated with feline (C) and canine (D) cells under the same conditions. The white arrows highlight filopodia without virus or Tf bound while the arrow in panel B shows virus concentrating on the filopodia of canine cells. (E) Time-lapse frames showing CPV-2 particles bound to filopodia of Cf2Th cells containing microinjected Alexa Fluor 488-actin. The tracks show particle movement on the filopodia; the yellow arrow indicates one particle moving toward the cell at the same rate as filopodial retraction. (F) Binding and uptake of CPV-2 capsids or canine Tf into Cf2Th cells expressing actin-GFP. In each field one cell has been injected with an antibody against the cytoplasmic tail of the Tf (labeled). (G) Effect of rabbit antibody against the TfR ectodomain on the binding and uptake of CPV-2 capsids or canine Tf to Cf2Th cells. Binding and uptake were performed similarly for the antibody-treated and untreated cells, and the images were taken at similar levels of exposure and camera gain. t, time; α, anti.

A clear difference was seen between the surface distribution of labeled capsids on canine and feline cells. When incubated with CRFK cells, CPV-2 (Fig. 4A) and CPV-2b (data not shown) capsids bound and were taken up uniformly over the cell surface. In contrast, lower levels of CPV-2 or CPV-2b particles bound to canine cells, and after 5 to 15 min at 37°C, most of the bound capsids were associated with filopodia rather than the cell body (Fig. 4B) (CPV-2b data not shown). Under the same conditions Alexa Fluor 594-labeled Tf bound evenly over both the feline and canine cells (Fig. 4C and D), indicating that this pattern was not the result of altered receptor distribution. After Alexa Fluor 488-labeled actin was microinjected into cells, the CPV-2 particles bound to filopodia showed mostly random and bidirectional movement (Fig. 4E) and did not move at the 1.8 to 3.2 μm/min rate reported in other systems which engage the retrograde actin transport processes (32, 57). Nonetheless, capsids accumulated at the cell body, perhaps associated with the retraction of the filopodia, as seen for some particles (Fig. 4E). Within about 10 to 20 min most virus was lost from the filopodia and became localized in vesicles within the cell. The attachment to filopodia was controlled by the surface expression of the canine TfR. Either

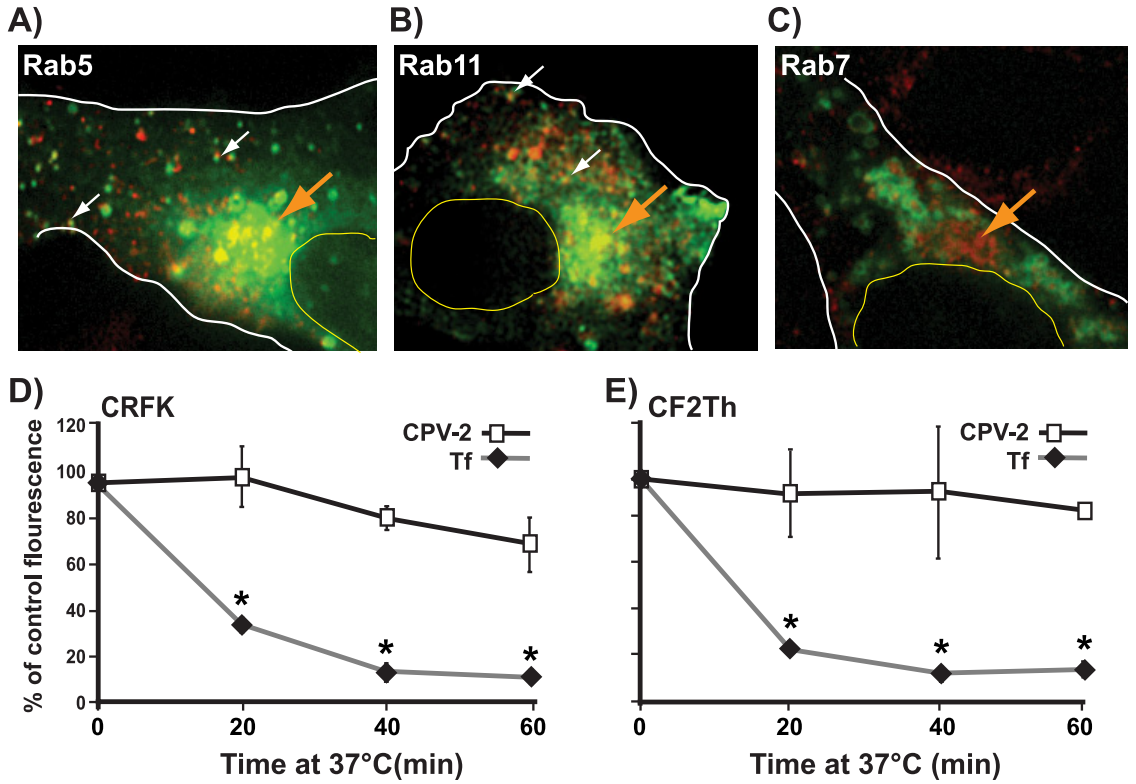

FIG. 5. Intracellular trafficking of labeled Tf (red) in CRFK cells containing GFP-Rab proteins (green) labeling different endosomal compartments. Colocalization is shown with Rab5 at 20 min (A) and Rab11 at 10 min (B) but not with Rab (27 min shown) (C). The large arrow highlights the perinuclear area, smaller vesicles showing colocalization are marked with small white arrows, and the cell body (white line) and nucleus (yellow line) are outlined. Retention and/or recycling of capsids or Tf to the cell surface was measured in CRFK (D) or Cf2Th (E) cells by the change in the level of fluorescently labeled ligand over time. (*, $P < 0.05$).

microinjection of an antibody recognizing the cytoplasmic sequence of the TfR (Fig. 4F) or the addition to the medium of antibody against the ectodomain of the TfR (Fig. 4G) greatly reduced or eliminated the attachment of the virus to the filopodia and capsid accumulation in the cell cytoplasm. The same treatments reduced but did not eliminate the binding of labeled Tf to the cells (Fig. 4F and G), most likely a reflection of the greater affinity of Tf for the remaining receptor on the cells.

Endosomal trafficking of Tf and viral capsids. As a control for the trafficking of virus in the cells expressing Rab-GFP constructs, we examined uptake and trafficking of Alexa Fluor 594-Tf and showed that it followed the endosomal pathways reported for Tf-TfR complexes (63). Tf first colocalized with Rab5-GFP in vesicles within 10 min of uptake (Fig. 5A) and with Rab11-GFP by 10 to 15 min (Fig. 5B). Little Tf colocalized with Rab7-GFP (Fig. 5C). Recycling in feline and canine cells also had similar dynamics to those described for Tf and TfR in human cells, with loss of cell-associated Tf within 20 to 30 min due to recycling to the cell surface and release (Fig. 5D and E) (10, 54). In contrast, the level of labeled virus associated with the cells decreased only slightly over 60 min of incubation, indicating that either capsids were retained within the recycling compartment or were diverted into other pathways where they persisted (Fig. 5D and E).

Soon after CPV-2 binding and uptake, particles were found within each of the three Rab-labeled endosomal compartments examined. Capsids colocalized and also showed comovement with Rab5-GFP-labeled vesicles as early as 5 min after uptake (Fig. 6A; see also Movie S1 in the supplemental material). At later times the association with Rab5 decreased although limited colocalization was still seen after ~1 h, particularly in cells showing high levels of Rab5-GFP expression (Fig. 6B). Expressing the CA Rab5-GFP resulted in the formation of large ring-shaped, Rab5-positive vesicles within the cells. Virus particles accumulated in these vesicles and were retained for prolonged periods (up to hours) after uptake. In some cases, particles were associated with the inner wall of the vesicles, while in others they released into the lumen (Fig. 6C; see also Movie S2 in the supplemental material). Trafficking patterns of the particles in canine Cf2Th cells expressing Rab5-GFP were similar to those seen in feline cells (Fig. 6D and E).

Within 15 to 20 min of uptake virus particles both colocalized and moved with Rab11- and Rab7-GFP vesicles (Fig. 7A and B). Movement of the virus-containing vesicles varied from stationary to very rapid and in some cases could not be accurately tracked even at frame rates of 0.2 s. Bidirectional movement, most likely on microtubules, was seen for virus-containing vesicles labeled with any of the Rab proteins examined. Within 30 to 45 min, the virus-containing vesicles accumulated in a perinuclear location near the microtubule organizing center. This area has high concentrations of both Rab11-positive (Fig. 7C and D) and Rab7-positive (Fig. 7E and F) vesicles, and in feline cells colocalization of capsids with particular

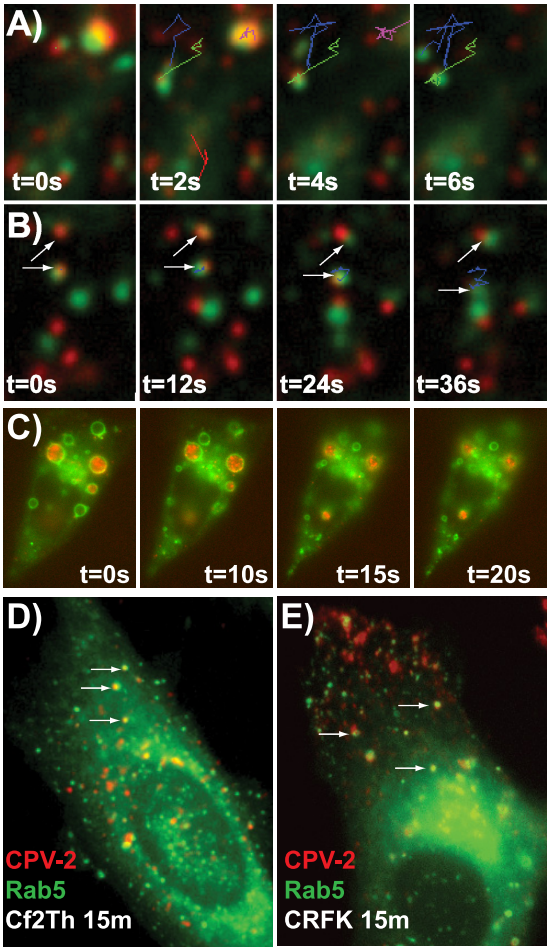

FIG. 6. The association of CPV-2 capsids with Rab5-GFP after endocytosis into cells. Time-lapse frames show the colocalization and comovement of Alexa Fluor 594-labeled capsids with wild-type Rab5-GFP in CRFK cells at 15 min (A) and 80 min (B). (C) CRFK cells expressing CA Rab5-GFP contain large vesicles that accumulate CPV-2 capsids (57 min after uptake). (D and E) Rab5-GFP expressed in Cf2Th or CRFK cells 15 min after virus uptake. Tracks of colocalized particles and vesicles are shown (A to C), while white arrows highlight colocalized virus and Rab5 (D and E). t, time.

markers was difficult even by confocal microscopy (results not shown).

Although viruses rapidly dispersed to multiple compartments after uptake in both feline and canine cells, some differences were seen in the intracellular distribution of virions. First, the patterns of accumulation at the perinuclear area differed. CRFK cells showed a tight accumulation of viral particles in vesicles (Fig. 7C and E),while in Cf2Th cells they clustered more loosely, and many endosomes appeared to contain several particles (Fig. 7D and F). In canine cells, colocalization of these groups of particles with Rab7-positive vesicles could be more clearly identified. The pattern of virus association with Rab11 vesicles also differed between the two cell types. Clusters of Rab11-positive vesicles were seen near the cell periphery of both cell types (Fig. 7C and D); however, localization of virus within these peripheral or polar vesicles was seen only in feline cells. These results suggest subtle differences in the endosomal trafficking of virions in different cell types. Examining for transport of virus into the nucleus, we used confocal microscopy to examine the location of virus in CRFK or Cf2th cells expressing lamin-A/C (Fig. 7G and H). In both cases only very small numbers of viral particles were observed within the nucleus. However, it was relatively difficult to distinguish the virus that was truly intranuclear from that which appeared intranuclear because it had entered the invaginations of the nuclear membrane (17), and the nuclear accumulation of the capsids was inefficient.

Expression of constitutively active Rab11 (Fig. 8A) or Rab7 (Fig. 8B) showed virus colocalization patterns similar to those seen for the wild-type proteins. However, as shown in Fig. 6C, the CA Rab5 disrupted the accumulation of virus at the perinuclear area, and particles were retained within larger ring-shaped vesicles (see Movie S2 in the supplemental material). The DN Rab5 had variable effects on intracellular trafficking. Some cells appeared similar to the wild type, but most cells showed moderate disruption of the perinuclear concentration of the virus (Fig. 8C). The DN Rab7 largely prevented perinuclear concentration (Fig. 8D). Finally, expression of DN Rab11 did not disrupt accumulation of the virus at the perinuclear area (Fig. 8E), suggesting that virus becomes localized within the late endosome at this location. For CPV-2 capsids, these patterns were similar in both canine and feline cells (data for canine cells not shown). Capsid release into the cytoplasm was not readily observed in these studies, and, as mentioned, only a small proportion of the particles enter the nucleus.

Infection of cells expressing CA or DN Rab-GFP proteins showed that wild-type Rab-GFP proteins had little effect on infection rates while wild-type Rab7 increased the infection rate (Fig. 9). However, expressing DN or CA Rab5 mutants reduced infection by about 50% in the expressing cells, as did DN Rab7. CA and DN Rab11 expression did not significantly affect infection rates.

DISCUSSION

Here, we examine the TfR-dependent binding, uptake, trafficking, and infection of cells by parvoviruses and show natural differences in the steps involved in feline and canine cells. Parvovirus infection is a complex process, and the various parvoviruses and AAVs that have been examined bind many different receptors and have been reported to follow many different pathways with different dynamics (reviewed in references 15 and 25). These live-cell studies revealed the processes of binding and entry of CPV when two distinct versions of the TfR were used, starting around ~5 min after virus addition, and showed a much more rapid and less linear process of endosomal trafficking than has been previously suggested. Virus particles taken up by the TfR were clearly identified as being within both recycling and late endosomes as early as 10 to 15 min after uptake. Although increasing expression of the wild-type Rab proteins likely perturbs aspects of the endosomal system, the intracellular capsid distribution was generally similar to that seen in cells fixed and stained for endosomal markers, and infection in cells expressing those proteins was not reduced. The behavior of Tf in cells expressing wild-type Rab-GFP has been examined in many studies and shows trafficking comparable to that seen in normal cells (29, 63). Even

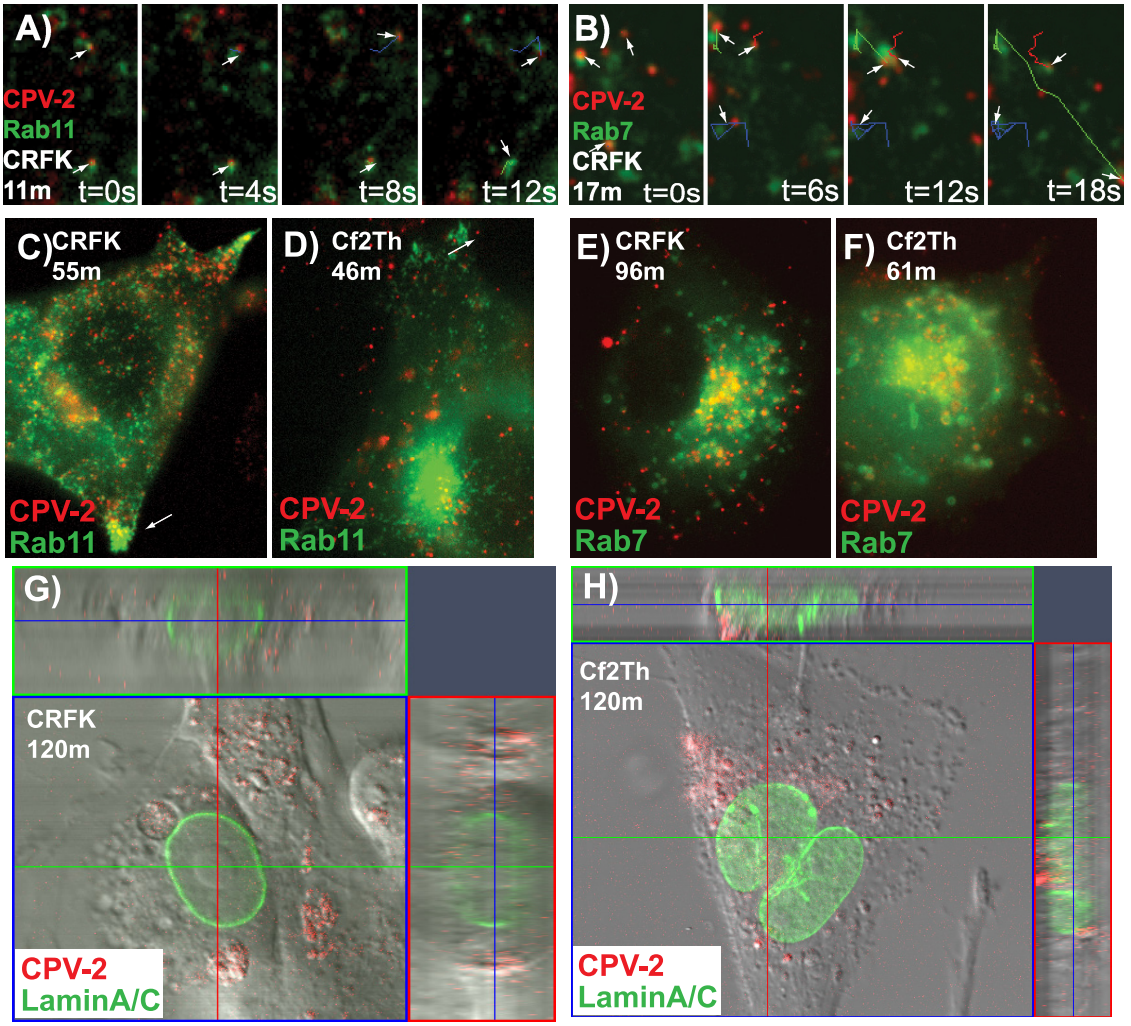

FIG. 7. Association of CPV-2 particles with Rab11-GFP or Rab7-GFP vesicles in cells after uptake. (A and B) Time-lapse frames of CPV-2 in feline CRFK cells expressing Rab11-GFP 11 min after uptake (A) and Rab7-GFP 17 min after uptake (B). Colocalization and comovement of some particles with labeled vesicles are highlighted as individual tracks. (C and D) Colocalization of virus with Rab11-GFP after uptake into CRFK cells for 55 min (C) or Cf2th cells for 46 min (D). The white arrows highlight polar accumulations of Rab11-positive vesicles. (E and F) Colocalization of virus with Rab7-GFP after uptake into CRFK cells at 96 min or Cf2th cells at 61 min. (G and H) Examining for nuclear localization of CPV capsids that entered CRFK or Cf2th cells expressing lamin-A/C-GFP. Confocal analysis shows cells and a section through the nucleus (at the level of the blue line), as well as two Z-sections (along the red and green lines) in each case. t, time.

when the CA Rab5 is expressed in cells, endocytic trafficking continues with some efficiency (10).

Binding and endocytosis. Although the levels of TfR expression in feline and canine cells were similar as detected by Tf or antibody binding, CPV capsids bound to canine cells at much lower levels due to their much lower affinity of binding. The infection efficiencies for canine cells differed for the different, naturally variant CPV strains. The CPV-2a/b variants first emerged in 1979, and these quickly replaced the original CPV-2 in dogs worldwide (48). These viruses differ antigenically and in their ability to infect and replicate in cats (66) and also in binding to the feline and canine cells and to the purified TfRs in vitro (42). Despite these differences, these viruses were seen here to be similar in surface and intracellular trafficking.

The uptake of infecting CPV from the surface of canine cells was delayed compared to that seen on feline cells, and this is likely to be due to both the lower affinity of the canine TfR and the interactions with filopodia before endocytosis. Filopodia are dynamic structures that contain actin bundles covered in membrane and are prominent at the leading edges of mobile cells (28). In tissue culture cells they present a large surface area and would therefore be of particular benefit for low-affinity interactions. The filopodial binding of CPV on canine cells was not a result of differences in receptor distribution as labeled canine Tf bound evenly over these cells. Binding and cellular uptake were associated with the TfR as it was inhibited by anti-TfR antibodies against either the cytoplasmic tail or the ectodomain (Fig. 4). The antibodies bind and cross-link the receptor, preventing correct trafficking and recycling, so that they greatly reduce TfR expression on the cell surface (44, 73). Capsids of a number of viruses bind preferentially to filopodia on cells, including retroviruses, papillomaviruses, and AAVs, and some are actively trafficked to the cell body by retrograde actin flow and/or myosin II acting on actin filaments (3, 32, 57).

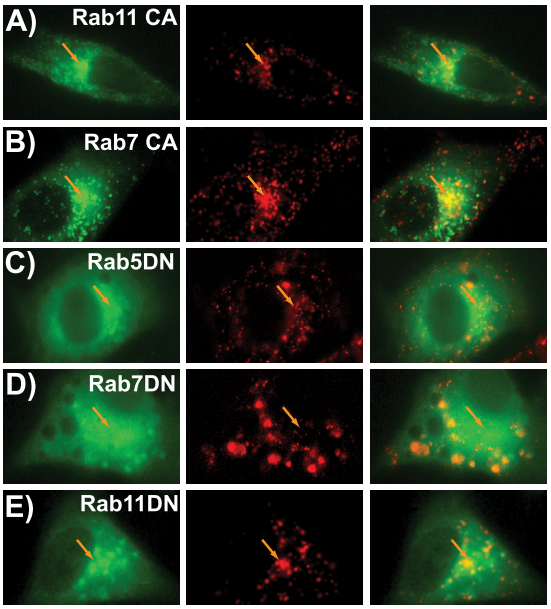

FIG. 8. Distribution of CPV-2 particles in CRFK cells expressing CA or DN Rab-GFP mutants. The individual Rab-GFP (green) and CPV-2 (red) channels are shown as well as the merged image. (A) CPV-2 capsids in cells expressing CA Rab11-GFP (35 min after uptake) or (B) CA Rab7-GFP (39 min) showing similar behavior to the wild type. (C) DN Rab5-GFP (43 min) showing limited disruption of the perinuclear virus concentration. (D) DN Rab7-GFP (50 min) caused an extensive redistribution of virus-containing vesicles. (E) Virus in cells expressing DN Rab11-GFP (59 min after uptake). Orange arrows highlight the perinuclear area in all cells.

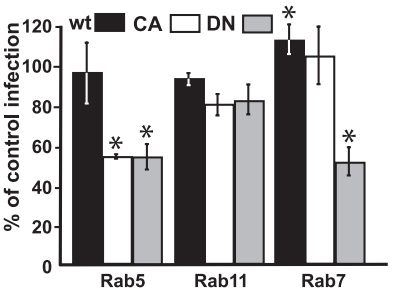

FIG. 9. The effect on FPV cell infection of wild-type (wt) and dominant negative Rab5-, Rab11- and Rab7-GFP expression. The percentages of cells expressing mutant Rab-GFP proteins that became infected by FPV compared to infection rates of nontransfected cells are shown (*, $P < 0.05$).

No consistent directional movement was seen for CPV particles on the filopodia of canine cells, but the bound virions accumulated at the base of these structures and entered the cells, at least in part due to the normal dynamic movement of the filopodia. We saw no evidence that CPV capsids induced the formation of filopodia or modified their behavior (62).

Binding and entry via the cell surface or filopodia allowed similar efficiencies of CPV-2 infection of both feline and canine cells while lower CPV-2b infection rates were seen in the canine cells. The efficient endocytosis by the TfR likely allows entry even for low-affinity interactions. TfR binding appears to provide a structural interaction necessary for infection as replacement of the TfR ectodomain with binding domains of antiviral antibodies allowed attachment and uptake of virus but not infection (26).

Endosomal trafficking. Within a few minutes of uptake, capsids were colocalized with Rab5-positive vesicles. Early endosomes are important in the initial sorting of many endocytosed cargoes into their correct endosomal pathways, a process that depends both on the cargo and the receptors (29, 59). The CA form of Rab5 induces large, ring-like vesicles in cells (10, 16), and a high proportion of the CPV particles entered these expanded vesicles and remained there for extended periods of 1 h or more (Fig. 6C). Many of these particles remained attached to the wall of the vesicle, probably as a result of their remaining attached to receptors. This confirms models showing prolonged interactions and slow trafficking, as was also seen by the microinjection of antibodies against the cytoplasmic tail of the TfR, which can block virus infection even when antibodies are injected 1 to 2 h after inoculation (44). The DN Rab5 also disrupted normal trafficking of the virus to the perinuclear region in many cells, again suggesting that the early endosome is required for correct endosomal trafficking, and reduced infectivity was seen in these cells.

Virus capsids were localized in both Rab11 and Rab7 vesicles by 15 min of uptake, a more rapid and complex trafficking of virus than previously suggested (64, 65). This trafficking would also be different from that of monomeric Tf. The icosahedral virus and dimeric TfR would result in cross-linked TfR-capsid complexes, which would be at least partly diverted into the degradative pathway (35). Even with limited cross-linking, the large virus capsid may alter trafficking within the tubular-vesicular endosomal sorting structures (6, 59).

Parvoviruses have been suggested to escape from the endosome along the degradative pathway (18, 34), and this view was supported by the finding that DN Rab7-GFP significantly decreased infection. Because the viruses require cell division for genome replication, expression of DN Rab proteins may disrupt the intracellular environment to indirectly inhibit replication. However, the mutants that disrupt the accumulation of virus at the perinuclear area showed the largest decreases in infection rates, suggesting a specific role for this trafficking in infection.

The entry of viruses into cells by receptor-mediated endocytosis can involve a variety of routes, and even for the parvoviruses receptors of many types are used for functional entry. These studies show that these viruses can efficiently use canine and feline TfRs with very different affinities of binding and initially follow different routes of uptake from the surface of feline and canine cells but then converge on the same vesicular compartments. This shows that the infection process can accommodate significant flexibility. In the case of CPV, binding to the canine TfR resulted in the host range shift from cats to dogs, and changes in TfR binding also resulted from the subsequent evolution in dogs. By examining the details of the interaction and trafficking events leading to infection, we can define the essential properties of the capsid and its interaction with the receptor and the cell entry pathways allowing efficient cell infection.

ACKNOWLEDGMENTS

Virginia Scarpino provided excellent technical support.

This study was supported by grants AI 28385 and AI 33468 from the National Institutes of Health to C.R.P.

REFERENCES

1. **Agbandje, M., R. McKenna, M. G. Rossmann, M. L. Strassheim, and C. R. Parrish.** 1993. Structure determination of feline panleukopenia virus empty particles. Proteins **16:**155–171.
2. **Aisen, P.** 2004. Transferrin receptor 1. Int. J. Biochem. Cell Biol. **36:**2137–2143.
3. **Bantel-Schaal, U., I. Braspenning-Wesch, and J. Kartenbeck.** 2009. Adeno-associated virus type 5 exploits two different entry pathways in human embryo fibroblasts. J. Gen. Virol. **90:**317–322.
4. **Bates, G. W., and M. R. Schlabach.** 1973. The reaction of ferric salts with transferrin. J. Biol. Chem. **248:**3228–3232.
5. **Bennett, M. J., J. A. Lebron, and P. J. Bjorkman.** 2000. Crystal structure of the hereditary haemochromatosis protein HFE complexed with transferrin receptor. Nature **403:**46–53.
6. **Bishop, N. E.** 2003. Dynamics of endosomal sorting. Int. Rev. Cytol. **232:**1–57.
7. **Brandenburg, B., L. Y. Lee, M. Lakadamyali, M. J. Rust, X. Zhuang, and J. M. Hogle.** 2007. Imaging poliovirus entry in live cells. PLoS Biol. **5:**e183.
8. **Brandenburg, B., and X. Zhuang.** 2007. Virus trafficking—learning from single-virus tracking. Nat. Rev. Microbiol. **5:**197–208.
9. **Campbell, E. M., and T. J. Hope.** 2008. Live cell imaging of the HIV-1 life cycle. Trends Microbiol. **16:**580–587.
10. **Ceresa, B. P., M. Lotscher, and S. L. Schmid.** 2001. Receptor and membrane recycling can occur with unaltered efficiency despite dramatic Rab5(q79l)-induced changes in endosome geometry. J. Biol. Chem. **276:**9649–9654.
11. **Cheng, Y., O. Zak, P. Aisen, S. C. Harrison, and T. Walz.** 2004. Structure of the human transferrin receptor-transferrin complex. Cell **116:**565–576.
12. **Coyne, C. B., and J. M. Bergelson.** 2006. Virus-induced Abl and Fyn kinase signals permit coxsackievirus entry through epithelial tight junctions. Cell **124:**119–131.
13. **Decaro, N., C. Desario, A. Parisi, V. Martella, A. Lorusso, A. Miccolupo, V. Mari, M. L. Colaianni, A. Cavalli, L. Di Trani, and C. Buonavoglia.** 2009. Genetic analysis of canine parvovirus type 2c. Virology **385:**5–10.
14. **Del Conte-Zerial, P., L. Brusch, J. C. Rink, C. Collinet, Y. Kalaidzidis, M. Zerial, and A. Deutsch.** 2008. Membrane identity and GTPase cascades regulated by toggle and cut-out switches. Mol. Syst. Biol. **4:**206.
15. **Ding, W., L. Zhang, Z. Yan, and J. F. Engelhardt.** 2005. Intracellular trafficking of adeno-associated viral vectors. Gene Ther. **12:**873–880.
16. **Dinneen, J. L., and B. P. Ceresa.** 2004. Continual expression of Rab5(Q79L) causes a ligand-independent EGFR internalization and diminishes EGFR activity. Traffic **5:**606–615.
17. **Ellenberg, J., E. D. Siggia, J. E. Moreira, C. L. Smith, J. F. Presley, H. J. Worman, and J. Lippincott-Schwartz.** 1997. Nuclear membrane dynamics and reassembly in living cells: targeting of an inner nuclear membrane protein in interphase and mitosis. J. Cell Biol. **138:**1193–1206.
18. **Farr, G. A., S. F. Cotmore, and P. Tattersall.** 2006. VP2 cleavage and the leucine ring at the base of the fivefold cylinder control pH-dependent externalization of both the VP1 N terminus and the genome of minute virus of mice. J. Virol. **80:**161–171.
19. **Farr, G. A., L. G. Zhang, and P. Tattersall.** 2005. Parvoviral virions deploy a capsid-tethered lipolytic enzyme to breach the endosomal membrane during cell entry. Proc. Natl. Acad. Sci. USA **102:**17148–17153.
20. **Fuchs, H., U. Lucken, R. Tauber, A. Engel, and R. Gessner.** 1998. Structural model of phospholipid-reconstituted human transferrin receptor derived by electron microscopy. Structure **6:**1235–1243.
21. **Gagescu, R., N. Demaurex, R. G. Parton, W. Hunziker, L. A. Huber, and J. Gruenberg.** 2000. The recycling endosome of Madin-Darby canine kidney cells is a mildly acidic compartment rich in raft components. Mol. Biol. Cell **11:**2775–2791.
22. **Giannetti, A. M., P. M. Snow, O. Zak, and P. J. Bjorkman.** 2003. Mechanism for multiple ligand recognition by the human transferrin receptor. PLoS Biol. **1:**E51.
23. **Hafenstein, S., L. M. Palermo, V. A. Kostyuchenko, C. Xiao, M. C. Morais, C. D. Nelson, V. D. Bowman, A. J. Battisti, P. R. Chipman, C. R. Parrish, and M. G. Rossmann.** 2007. Asymmetric binding of transferrin receptor to parvovirus capsids. Proc. Natl. Acad. Sci. USA **104:**6585–6589.
24. **Hao, M., and F. R. Maxfield.** 2000. Characterization of rapid membrane internalization and recycling. J. Biol. Chem. **275:**15279–15286.
25. **Harbison, C. E., J. A. Chiorini, and C. R. Parrish.** 2008. The parvovirus capsid odyssey: from the cell surface to the nucleus. Trends Microbiol. **16:**208–214.
26. **Hueffer, K., L. M. Palermo, and C. R. Parrish.** 2004. Parvovirus infection of cells by using variants of the feline transferrin receptor altering clathrin-mediated endocytosis, membrane domain localization, and capsid-binding domains. J. Virol. **78:**5601–56011.
27. **Hueffer, K., J. S. Parker, W. S. Weichert, R. E. Geisel, J. Y. Sgro, and C. R. Parrish.** 2003. The natural host range shift and subsequent evolution of canine parvovirus resulted from virus-specific binding to the canine transferrin receptor. J. Virol. **77:**1718–1726.
28. **Kaksonen, M., C. P. Toret, and D. G. Drubin.** 2006. Harnessing actin dynamics for clathrin-mediated endocytosis. Nat. Rev. Mol. Cell Biol. **7:**404–414.
29. **Lakadamyali, M., M. J. Rust, and X. Zhuang.** 2006. Ligands for clathrin-mediated endocytosis are differentially sorted into distinct populations of early endosomes. Cell **124:**997–1009.
30. **Lau, C., X. Wang, L. Song, M. North, S. Wiehler, D. Proud, and C. W. Chow.** 2008. Syk associates with clathrin and mediates phosphatidylinositol 3-kinase activation during human rhinovirus internalization. J. Immunol. **180:**870–880.
31. **Lawrence, C. M., S. Ray, M. Babyonyshev, R. Galluser, D. W. Borhani, and S. C. Harrison.** 1999. Crystal structure of the ectodomain of human transferrin receptor. Science **286:**779–782.
32. **Lehmann, M. J., N. M. Sherer, C. B. Marks, M. Pypaert, and W. Mothes.** 2005. Actin- and myosin-driven movement of viruses along filopodia precedes their entry into cells. J. Cell Biol. **170:**317–325.
33. **Lux, K., N. Goerlitz, S. Schlemminger, L. Perabo, D. Goldnau, J. Endell, K. Leike, D. M. Kofler, S. Finke, M. Hallek, and H. Buning.** 2005. Green fluorescent protein-tagged adeno-associated virus particles allow the study of cytosolic and nuclear trafficking. J. Virol. **79:**11776–11787.
34. **Mani, B., C. Baltzer, N. Valle, J. M. Almendral, C. Kempf, and C. Ros.** 2006. Low pH-dependent endosomal processing of the incoming parvovirus minute virus of mice virion leads to externalization of the VP1 N-terminal sequence (N-VP1), N-VP2 cleavage, and uncoating of the full-length genome. J. Virol. **80:**1015–1024.
35. **Marsh, E. W., P. L. Leopold, N. L. Jones, and F. R. Maxfield.** 1995. Oligomerized transferrin receptors are selectively retained by a lumenal sorting signal in a long-lived endocytic recycling compartment. J. Cell Biol. **129:**1509–1522.
36. **Marsh, M., and A. Helenius.** 2006. Virus entry: open sesame. Cell **124:**729–740.
37. **Maxfield, F. R., and T. E. McGraw.** 2004. Endocytic recycling. Nat. Rev. Mol. Cell Biol. **5:**121–132.
38. **McCaffrey, M. W., A. Bielli, G. Cantalupo, S. Mora, V. Roberti, M. Santillo, F. Drummond, and C. Bucci.** 2001. Rab4 affects both recycling and degradative endosomal trafficking. FEBS Lett. **495:**21–30.
39. **McGraw, T. E., L. Greenfield, and F. R. Maxfield.** 1987. Functional expression of the human transferrin receptor cDNA in Chinese hamster ovary cells deficient in endogenous transferrin receptor. J. Cell Biol. **105:**207–214.
40. **Nelson, C. D., E. Minkkinen, M. Bergkvist, K. Hoelzer, M. Fisher, B. Bothner, and C. R. Parrish.** 2008. Detecting small changes and additional peptides in the canine parvovirus capsid structure. J. Virol. **82:**10397–10407.
41. **Odorizzi, G., A. Pearse, D. Domingo, I. S. Trowbridge, and C. R. Hopkins.** 1996. Apical and basolateral endosomes of MDCK cells are interconnected and contain a polarized sorting mechanism. J. Cell Biol. **135:**139–152.
42. **Palermo, L. M., S. L. Hafenstein, and C. R. Parrish.** 2006. Purified feline and canine transferrin receptors reveal complex interactions with the capsids of canine and feline parvoviruses that correspond to their host ranges. J. Virol. **80:**8482–8492.
43. **Palermo, L. M., K. Hueffer, and C. R. Parrish.** 2003. Residues in the apical domain of the feline and canine transferrin receptors control host-specific binding and cell infection of canine and feline parvoviruses. J. Virol. **77:**8915–8923.
44. **Parker, J. S., W. J. Murphy, D. Wang, S. J. O'Brien, and C. R. Parrish.** 2001. Canine and feline parvoviruses can use human or feline transferrin receptors to bind, enter, and infect cells. J. Virol. **75:**3896–3902.
45. **Parker, J. S., and C. R. Parrish.** 2000. Cellular uptake and infection by canine parvovirus involves rapid dynamin-regulated clathrin-mediated endocytosis, followed by slower intracellular trafficking. J. Virol. **74:**1919–1930.
46. **Parker, J. S. L., and C. R. Parrish.** 1997. Canine parvovirus host range is determined by the specific conformation of an additional region of the capsid. J. Virol. **71:**9214–9222.
47. **Parrish, C. R.** 1991. Mapping specific functions in the capsid structure of canine parvovirus and feline panleukopenia virus using infectious plasmid clones. Virology **183:**195–205.
48. **Parrish, C. R., C. Aquadro, M. L. Strassheim, J. F. Evermann, J.-Y. Sgro, and H. Mohammed.** 1991. Rapid antigenic-type replacement and DNA sequence evolution of canine parvovirus. J. Virol. **65:**6544–6552.
49. **Parrish, C. R., P. Have, W. J. Foreyt, J. F. Evermann, M. Senda, and L. E. Carmichael.** 1988. The global spread and replacement of canine parvovirus strains. J. Gen. Virol. **69:**1111–1116.
50. **Parrish, C. R., and Y. Kawaoka.** 2005. The origins of new pandemic viruses: the acquisition of new host ranges by canine parvovirus and influenza A viruses. Annu. Rev. Microbiol. **59:**553–586.
51. **Pietiainen, V., V. Marjomaki, P. Upla, L. Pelkmans, A. Helenius, and T. Hyypia.** 2004. Echovirus 1 endocytosis into caveosomes requires lipid rafts, dynamin II, and signaling events. Mol. Biol. Cell **15:**4911–4925.
52. **Radoshitzky, S. R., J. Abraham, C. F. Spiropoulou, J. H. Kuhn, D. Nguyen, W. Li, J. Nagel, P. J. Schmidt, J. H. Nunberg, N. C. Andrews, M. Farzan, and**

H. Choe. 2007. Transferrin receptor 1 is a cellular receptor for New World haemorrhagic fever arenaviruses. Nature **446:**92–96.
53. **Rappoport, J. Z.** 2008. Focusing on clathrin-mediated endocytosis. Biochem. J. **412:**415–423.
54. **Ren, M., G. Xu, J. Zeng, C. De Lemos-Chiarandini, M. Adesnik, and D. D. Sabatini.** 1998. Hydrolysis of GTP on Rab11 is required for the direct delivery of transferrin from the pericentriolar recycling compartment to the cell surface but not from sorting endosomes. Proc. Natl. Acad. Sci. USA **95:**6187–6192.
55. **Robinson, M. S.** 2004. Adaptable adaptors for coated vesicles. Trends Cell Biol. **14:**167–174.
56. **Ross, S. R., J. J. Schofield, C. J. Farr, and M. Bucan.** 2002. Mouse transferrin receptor 1 is the cell entry receptor for mouse mammary tumor virus. Proc. Natl. Acad. Sci. USA **99:**12386–12390.
57. **Schelhaas, M., H. Ewers, M. L. Rajamaki, P. M. Day, J. T. Schiller, and A. Helenius.** 2008. Human papillomavirus type 16 entry: retrograde cell surface transport along actin-rich protrusions. PLoS Pathog. **4:**e1000148.
58. **Seaman, M. N.** 2008. Endosome protein sorting: motifs and machinery. Cell. Mol. Life Sci. **65:**2842–2858.
59. **Sharma, M., F. Pampinella, C. Nemes, M. Benharouga, J. So, K. Du, K. G. Bache, B. Papsin, N. Zerangue, H. Stenmark, and G. L. Lukacs.** 2004. Misfolding diverts CFTR from recycling to degradation: quality control at early endosomes. J. Cell Biol. **164:**923–933.
60. **Simpson, A. A., V. Chandrasekar, B. Hebert, G. M. Sullivan, M. G. Rossmann, and C. R. Parrish.** 2000. Host range and variability of calcium binding by surface loops in the capsids of canine and feline parvoviruses. J. Mol. Biol. **300:**597–610.
61. **Smith, A. E., and A. Helenius.** 2004. How viruses enter animal cells. Science **304:**237–242.
62. **Smith, J. L., D. S. Lidke, and M. A. Ozbun.** 2008. Virus activated filopodia promote human papillomavirus type 31 uptake from the extracellular matrix. Virology **381:**16–21.
63. **Sonnichsen, B., S. De Renzis, E. Nielsen, J. Rietdorf, and M. Zerial.** 2000. Distinct membrane domains on endosomes in the recycling pathway visualized by multicolor imaging of Rab4, Rab5, and Rab11. J. Cell Biol. **149:**901–914.
64. **Suikkanen, S., M. Antila, A. Jaatinen, M. Vihinen-Ranta, and M. Vuento.** 2003. Release of canine parvovirus from endocytic vesicles. Virology **316:**267–280.
65. **Suikkanen, S., K. Saajarvi, J. Hirsimaki, O. Valilehto, H. Reunanen, M. Vihinen-Ranta, and M. Vuento.** 2002. Role of recycling endosomes and lysosomes in dynein-dependent entry of canine parvovirus. J. Virol. **76:**4401–4411.
66. **Truyen, U., A. Gruenberg, S. F. Chang, B. Obermaier, P. Veijalainen, and C. R. Parrish.** 1995. Evolution of the feline-subgroup parvoviruses and the control of canine host range in vivo. J. Virol. **69:**4702–4710.
67. **Truyen, U., and C. R. Parrish.** 1992. Canine and feline host ranges of canine parvovirus and feline panleukopenia virus: distinct host cell tropisms of each virus in vitro and in vivo. J. Virol. **66:**5399–5408.
68. **Tsao, J., M. S. Chapman, M. Agbandje, W. Keller, K. Smith, H. Wu, M. Luo, T. J. Smith, M. G. Rossmann, R. W. Compans, and C. R. Parrish.** 1991. The three-dimensional structure of canine parvovirus and its functional implications. Science **251:**1456–1464.
69. **Van Dam, E. M., and W. Stoorvogel.** 2002. Dynamin-dependent transferrin receptor recycling by endosome-derived clathrin-coated vesicles. Mol. Biol. Cell **13:**169–182.
70. **Van Dam, E. M., T. Ten Broeke, K. Jansen, P. Spijkers, and W. Stoorvogel.** 2002. Endocytosed transferrin receptors recycle via distinct dynamin and phosphatidylinositol 3-kinase-dependent pathways. J. Biol. Chem. **277:**48876–48883.
71. **van der Schaar, H. M., M. J. Rust, C. Chen, H. van der Ende-Metselaar, J. Wilschut, X. Zhuang, and J. M. Smit.** 2008. Dissecting the cell entry pathway of dengue virus by single-particle tracking in living cells. PLoS Pathog. **4:**e1000244.
72. **Vihinen-Ranta, M., D. Wang, W. S. Weichert, and C. R. Parrish.** 2002. The VP1 N-terminal sequence of canine parvovirus affects nuclear transport of capsids and efficient cell infection. J. Virol. **76:**1884–1891.
73. **White, S., K. Miller, C. Hopkins, and I. S. Trowbridge.** 1992. Monoclonal antibodies against defined epitopes of the human transferrin receptor cytoplasmic tail. Biochim. Biophys. Acta **1136:**28–34.
74. **Yeung, D. E., G. W. Brown, P. Tam, R. H. Russnak, G. Wilson, I. Clark-Lewis, and C. R. Astell.** 1991. Monoclonal antibodies to major nonstructural nuclear protein of minute virus of mice. Virology **181:**35–45.
75. **Zadori, Z., J. Szelei, M.-C. Lacoste, P. Raymond, M. Allaire, I. R. Nabi, and P. Tijssen.** 2001. A viral phospholipase A2 is required for parvovirus infectivity. Dev. Cell **1:**291–302.